Improved LLS imaging performance in scattering-dominant waters

Fraser R. Dalgleish, Frank M. Caimi, Walter B. Britton and Carl F. Andren
Florida Atlantic Univ./Harbor Branch, 5600 US 1, Fort Pierce, FL, USA 34946

ABSTRACT

Experimental results from two alternate approaches to underwater imaging based around the well known Laser Line Scan (LLS) serial imaging technique are presented. Traditionally employing Continuous Wave (CW) laser excitation, LLS is known to improve achievable distance and image contrast in scattering-dominant waters by reducing both the backscatter and forward scatter levels reaching the optical receiver. This study involved designing and building prototype benchtop CW-LLS and pulsed-gated LLS imagers to perform a series of experiments in the Harbor Branch Oceanographic Institute (HBOI) full-scale laser imaging tank, under controlled scattering conditions using known particle suspensions. Employing fixed laser-receiver separation (24.3cm) in a bi-static optical geometry, the CW-LLS was capable of producing crisp, high contrast images at beyond 4 beam attenuation lengths at 7 meters stand-off distance. Beyond this stand-off distance or at greater turbidity, the imaging performance began to be limited mainly by multiple backscatter and shot noise generated in the receiver, eventually reaching a complete contrast limit at around 6 beam attenuation lengths. Using identical optical geometry as the CW-LLS, a pulsed-gated laser line scan (PG-LLS) system was configured and tested, demonstrating a significant reduction in the backscatter reaching the receiver. When compared with the CW-LLS at 7 meters stand-off distance, the PG-LLS did not become limited due to multiple backscatter, instead reaching a limit (believed to be primarily due to forward-scattered light overcoming the attenuated direct target signal) beyond 7 beam attenuation lengths. This result demonstrates the potential for a greater operational limit as compared to previous CW-LLS configuration.

Keywords: laser imaging, underwater imaging, range-gated, Lidar, image quality

1. INTRODUCTION

Obtaining identification-quality optical images from the underwater environment is an important requirement in military, commercial and scientific operations. Increases in particle concentration within the water column will cause volumetric light scattering both from sunlight and from artificial illumination, and this can lead to images being of a lower quality than that required for identification. Several approaches are currently used which reduce the main mechanisms responsible for the loss in image quality.

Laser Line Scan (LLS) underwater imaging is a serial imaging technique which involves the optical scanning of a narrow instantaneous field of view (IFOV) receiver in a synchronous fashion with a highly collimated laser source over a wide swath. It is widely regarded as the optimal technology for extended range underwater optical imaging, with up to 6 attenuation lengths achievable in turbid sea water [1][2][3][4]. These imagers, which typically utilize moderate-power green continuous wave (CW) lasers, require an adequate laser-receiver separation to reduce the imaging detriment of near-field multiple backscatter. Currently available systems are large and require too much power to make them suitable for modern unmanned underwater platforms such as the man-portable autonomous underwater vehicle (AUV). For compact implementations of CW-LLS, the detection of target signals becomes obstructed by temporal overlap from backscatter levels in turbid water. To increase their operational range and provide high quality identification-quality imagery, detection methods must be capable of separating the target and scattering signals to estimate the energy returning from the target alone. Over-sampling techniques, which average many samples for each image pixel, can be used to increase signal to noise ratio and hence improve image contrast, albeit with a reduction of image resolution due to intra-pixel scan and platform motion. Intensity modulation of the CW laser with coherent processing at the detection stage offers some promise in improving contrast and providing bathymetric imaging capabilities from modulation phase

Ocean Sensing and Monitoring, edited by Weilin (Will) Hou, Proc. of SPIE Vol. 7317, 73170E

information, but in the presence of high levels of backscatter the shot noise levels being generated in the receiver increase to the point where the system becomes contrast limited [5].

The other main technique used for extended range underwater imaging system is that of range-gating, where the temporal aspects of the source and receiver are precisely synchronized using a pulsed laser, gated or time discriminating receiver, and knowledge of the time of arrival of the target signal. These methods also have the potential to determine bathymetry from the travel time of the light pulses, and from a system packaging perspective, pulsed-gated imager architectures are amenable to a more compact implementation with a reduced laser-receiver separation being possible. Such techniques can allow separation of the target and scattering volume return signals, thereby increasing the imaging range possible under certain conditions. Several previous configurations using spatially broadened laser pulses and precise gated, intensified cameras were built and tested, with results indicating imaging performance beyond 6 beam attenuation lengths [4][6][7][8][9][10]. However, employing wide-angle array-style detectors, the systems are susceptible to image degradation due to multiple forward scatter in very turbid water, even when extremely short gate times are used. Furthermore these systems don't offer the wide swath (~70 degrees) imagery which LLS systems can provide.

Recent simulation work [11][12] has suggested that in scattering dominant waters, the PG-LLS will improve the achievable image contrast over the CW-LLS, as well as allow for more compact system implementations. To support this study, including the validation of image performance prediction simulation software, a prototype LLS system was demonstrated in the Florida Atlantic University/Harbor Branch Oceanographic Institute full-scale laser imaging tank under highly controlled conditions of scattering particle concentration (turbidity). Two distinct design alternatives were tested and compared: i) CW-LLS, i.e. the use of a CW laser and a non-gated photomultiplier tube (PMT); ii) PG-LLS, i.e. the use of a high repetition rate pulsed green laser and a custom gated-PMT. A series of experiments were conducted in the HBOI laser imaging test facility at realistic stand-off distances in a variety of turbidity conditions ranging from very clear conditions to greater than 7 attenuation lengths. Scattering was varied by the addition of Maalox: optical properties were measured with an ac-9 meter. The acquired images were analyzed using standard image quality metrics to compare the relative contrast and signal-noise ratios versus number of beam attenuation lengths for both the CW-LLS and PG-LLS.

2. BACKGROUND

In order to understand the potential for turbid water imaging performance improvement with the PG-LLS over the CW-LLS, it is necessary to examine the light collection process prior to formation of each pixel for a serial imaging system such as the LLS.

The objective of the LLS architecture is to suppress unwanted backscattered and forward-scattered light while still recovering the image-bearing photons. It accomplishes this by employing a synchronously-scanned collimated laser beam and narrow receiver field of view in a bi-static configuration. Figure 1 shows the LLS imaging geometry at a single instant during a line scan. It can be seen that many possible paths exist for both direct and scattered light to follow from being emitted from the laser source, to eventually returning to the receiver to form a component of the image. For the purpose of this simplified analysis, the returns from scattered and upwelling sunlight will not be considered.

Light which doesn't make it as far as the target, but is still gathered by the receiver is known as backscatter. As shown in figure 1, backscatter can be further categorized into light which either takes a multiply scattered shortcut to the receiver or light which is initially scattered in the common volume formed between the laser source and the instantaneous field of view (IFOV) of the receiver. Figure 2 illustrates this phenomena from measured pulse time history plots for both clear water and water with high particle concentration. The first broad return is due to multiple scattering from particles near the receiver, where the laser energy is greatest. This is followed by the narrower return from common volume backscatter, defined by the intersection of the receiver field-of-view with the laser beam. Finally, the reflection from the target in the object plane arrives at the receiver. The common volume backscatter peak occurs close to the onset of the common volume region since the intensity of the laser pulse falls off exponentially as it transits the common volume. At higher turbidities, the multiple backscatter return is significant and overlaps the common volume backscatter return.

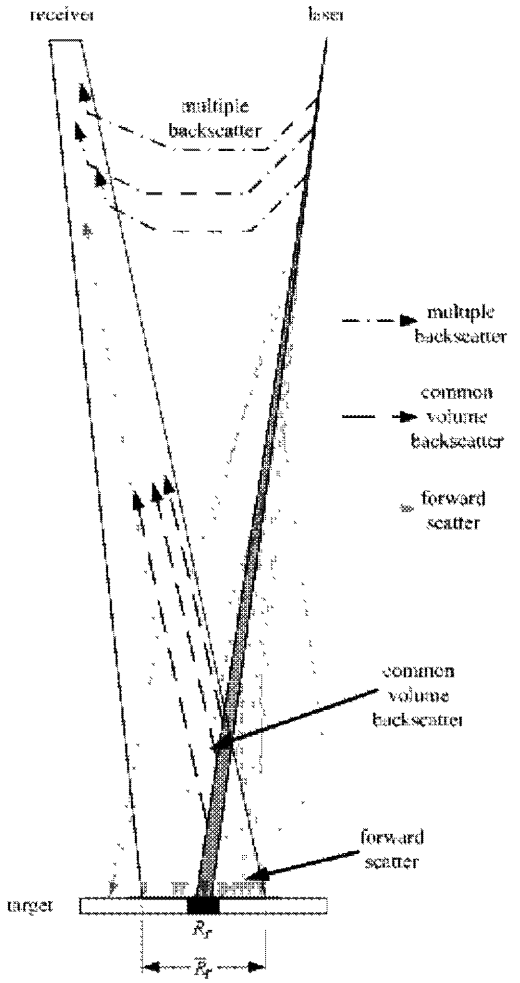

Figure 1. LLS imaging geometry at a single instant during a line scan, showing possible routes into the receiver aperture for defined categories of scattered and direct light

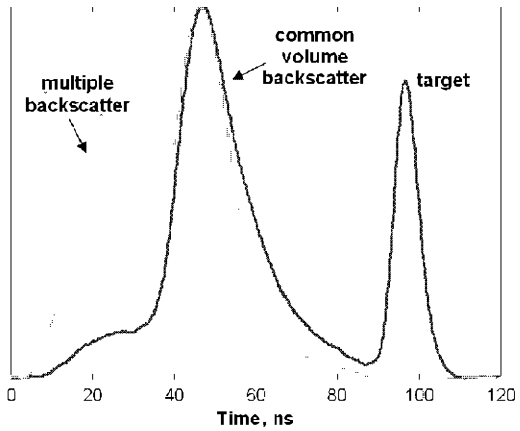

Figure 2. Representative normalized laser pulse time-history measurements for two turbidities. At the higher turbidity (lighter shade) the multiple backscatter peak is stronger and the target return is weaker.

The total backscatter irradiance collected by the receiver is defined as the backscatter component (E_{BS}). The effect of backscatter on an acquired image is a reduction in contrast and signal to noise ratio. Backscatter is independent of target reflectance and can be reduced by increasing the source-receiver separation, or decreasing the laser and receiver angular apertures. However, as the scattering particle concentration increases, multiple-scattered backscatter levels increase, eventually leading to the contrast limit for a CW-LLS system. The main objective of the PG-LLS described in this paper is to remove the backscatter component using electronic gating.

Not all the light received by a LLS system that has been reflected from the target contains useful information about the region of target being scanned at that instant in time. The component of the received light which has made it to the target, but which has undergone scattering with particles and water molecules on the outgoing path can be defined as the forward scattered component (E_{FS}). Carrying reflectance information from a larger region of the target $\bar{R}_T$ (shown in figure 1) the main effect of forward scatter on an acquired image is a reduction in resolution, contrast and signal to noise ratio, particularly when the surrounding target has a high mean reflectance and forward scatter appears as a blurring or glow. For the non-coherent, direct detection LLS systems being discussed in this paper, the only way to minimize forward scatter is to reduce laser and receiver angular apertures.

The image component that contains useful reflectance information from the small region of the target R_T (shown in figure 1), which is illuminated by the unscattered laser beam, is called the direct component (E_D). This consists of light which has not been scattered out of the main beam on the way to the target, but can consist of light which has undergone multiple small angle scattering on the way back from the target to the receiver, through those combinations of angles that allow acceptance into the receiver aperture.

2.1 CW-LLS Image Formation

It follows that each pixel formed by the CW-LLS consists of the linear superposition of all three components of returning light present at the receiver, i.e.

$$E(x,y)_{CW\text{-}LLS} = E(x,y)_{BS} + E(x,y)_{FS} + E(x,y)_{D} \quad (1)$$

The CW-LLS system will continuously integrate the total signal from the photomultiplier tube (PMT) over several microseconds for each image pixel. Longer integration times can improve signal to noise ratio when backscatter levels are high, but also lead to increased intra-pixel scan distance, and hence a reduction in spatial resolution.

2.2 PG-LLS Image formation

Utilizing electronic gating to remove the backscatter component, each pixel formed by the PG-LLS consists of the linear superposition of only the direct and forward-scattered components of returning light present at the receiver, i.e.

$$E(x,y)_{PG\text{-}LLS} = E(x,y)_{FS} + E(x,y)_{D} \quad (2)$$

For a particular stand-off distance, the PG-LLS system will use a constant delay between the pulse being emitted and the receiver gate being activated. Following a period of approximately 20ns for the PMT responsivity to reach a stable state, the target signal reaches the receiver and the system integrates over a fixed window which is determined *a priori* based on the expected target to receiver stand-off distance.

2.3 Image Quality Analysis

To compare imager performance it was necessary to use technical targets to compute image statistics and therefore analyze how image quality varied under different environmental and system parameters. The image analysis methods used in this study are contrast (equation 3) and contrast signal to noise ratio (equation 4) algorithms used with USAF-1951 targets. Both the white-on-black (WoB) and black-on-white (BoW) technical targets were used to explore the imager limitations under different levels of background reflectance and hence forward scatter.

Contrast ratio:
$$\frac{WhiteMean - BlackMean}{WhiteMean + BlackMean} \quad (3)$$

CSN ratio:
$$\frac{WhiteMean - BlackMean}{\sqrt{WhiteSTD^2 + BlackSTD^2}} \quad (4)$$

The targets were mounted on a drum which was rotated at a known speed (1 m/s) in order to form a 2D image. A section of the drum with the WoB technical target is shown in figure 3. The contrast ratios were computed for raw target images with means and standard deviations computed over adjacent 'black' and 'white' squares of the technical target (shown by overlaid squares on the cropped squares in figure 3). The computed values are used in section 4 to compare image quality between alternate tested configurations.

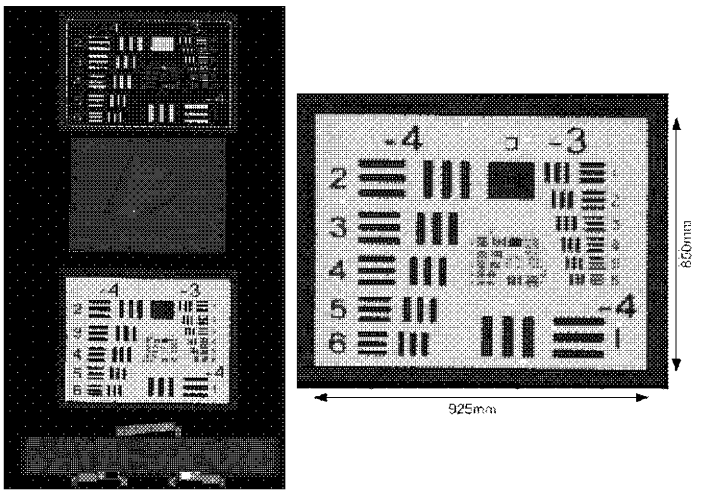

Figure 3. Left: LLS image of entire drum cycle. Right: cropped section of BoW technical target showing target dimensions and image quality analysis regions. The target reflectance was measured in air using a laser and fiber-coupled spectrometer pair at 532nm with Spectralon™ reflectance references. Black regions had a reflectance of 25% and white regions 65%.

3. EXPERIMENTAL CONFIGURATION

3.1 Test tank

Experiments were conducted at the large optical imaging test tank located at the Harbor Branch Oceanographic Institute (HBOI) campus of Florida Atlantic University in Fort Pierce, Florida. A photograph of the test tank, showing the rotating drum target is shown in figure 4. A benchtop single polygon LLS unit was used to synchronously scan the laser beam and narrow receiver IFOV over the target (figure 5). Data were collected at 7 meters stand-off distance for both LLS imaging configurations. The turbidity of the water in the tank was adjusted by adding a mixture of 50% laboratory grade Magnesium Hydroxide particles and 50% laboratory grade Aluminum Hydroxide particles. The resultant beam attenuation coefficient (c) and absorption coefficient (a) at 532nm were measured with a Wetlabs ac-9 transmissometer. Beam attenuation measurements were corrected for scattering errors as advised by the manufacturer. The single scattering albedo, defined as the scattering to beam attenuation coefficient ratio was observed to be > 90% for turbid conditions created. In previous tests, homogeneity of the measured c values at different locations and depths within the tank was verified 30 - 40 minutes after each addition. Images were taken with both LLS methods at c values of 0.09, 0.22, 0.44, 0.54, 0.65, 0.76, 0.87, 0.98 and 1.09 m^{-1}. The full set of image data at the various turbidities were first made with the CW-LLS configuration. The water in the tank was then filtered for several days, the ac-9 meter was cleaned, and the PG-LLS components were installed. Correct alignment was verified, and the turbidity cycling and image acquisition sequence was repeated.

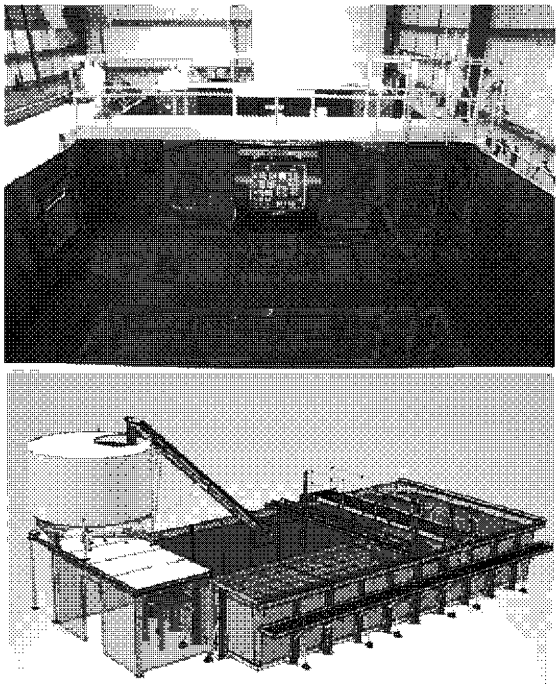

Figure 4. HBOI large optical imaging test tank. Top (photo of tank partially drained). Bottom (CAD model of tank).

3.2 Benchtop imaging hardware

Synchronous scanning optics

The scanning architecture used for comparing the performance of the CW-LLS and the PG-LLS in the HBOI extended range optical test facility is built around a single six-faceted polygonal scan mirror [13]. The objective is to have a narrow IFOV at the receiver channel which is optically coincident with the outgoing laser pulse throughout the entire scan angle for a fixed stand-off distance. For the tests described herein, the images were acquired over a total swath of less than 20 degrees. The laser output is folded by 90° along the beam entry axis towards the polygon, where it is deflected via the transmit steering mirror pair over the top of the polygon and through the optical port into the water. As the stand-off distance is adjusted, a mechanism to maintain this optical synchronization is required. The incorporation of two symmetrical steering mirror assemblies allows this to be accomplished. The laser-receiver separation at the viewport for the system is 23.4cm. Figure 5 shows the scanner concept together with a photo of the fabricated scanner.

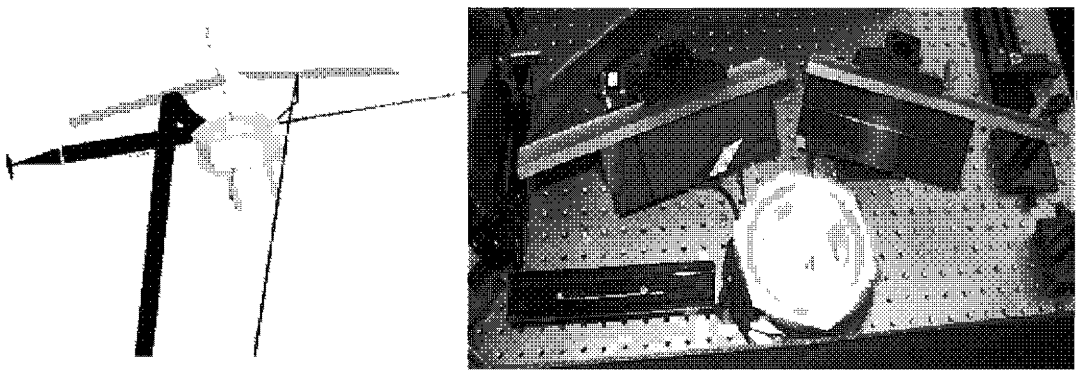

Figure 5. Left: Scanner concept illustrating rotating polygon scanner, steering mirrors and collection to small aperture detector. Right: Photo of scanner on optical bench.

Laser sources

For testing with the PG-LLS, a custom high repetition rate green (532nm) pulsed laser was developed by Q-Peak (Bedford, MA). This solid state amplified master oscillator Q-switched YAG laser produced 7ns FWHM green pulses at a fixed pulse repetition rate of 357KHz. The average power entering the water was 1.3W (4.6μJ average pulse energy) with pulse-to-pulse energy instability of up to 40%. The pulse-to-pulse timing jitter was typically 10-20 ns. A small portion of the output was sampled by a reference detector and was used as a pulse monitor, both to trigger the receiver gate electronics and for normalization of pulse-to-pulse energy variations in acquired images. The beam diameter was less than 2 mm with a far-field beam divergence of 2 mrad. A 2.2W green (532nm) CW laser (Melles Griot GHS-509) was used for the CW-LLS testing, also with 2 mrad beam divergence.

Receivers

The returning photons entering the optical port from the target are incident on the upper receive steering mirror, where they are deflected to the lower receiver steering mirror and onto another facet of the polygon, from which the light is directed towards a 90° folding mirror and into the receiver assembly, which consists of a 50mm diameter plano-convex focusing lens, an adjustable circular aperture, behind which is mounted a Hamamatsu R7600U photomultiplier tube (PMT) which has been configured to be electronically gateable by switching the first dynode on and off. For the CW-LLS tests, the R7600U was used in a continuous mode.

Sampling parameters

In this comparison an effort was made to match the energy delivered per pixel for each imaging configuration. The distance on the target swept for each image pixel (i,e, the theoretical spatial resolution) was kept as close as system hardware limitations would allow. The same scan speed was used for each imaging configuration (100 lines per second). The following table summarizes the laser energy delivered per pixel, integration time (for CW-LLS), pulse period (for PG-LLS) and the subsequent theoretical spatial resolution.

Table 1. Sampling parameters for LLS imaging comparison at 7 meters and 100 lines per second.

CW LLS		**PG LLS**	
Power (W)	Integration time (μs)	Mean Pulse Energy (μJ)	Pulse Repetition Period (μs)
2.2	2.1	4.6	2.8
Energy per pixel (μJ)	Spatial Resolution (mm)	Energy per pixel (μJ)	Spatial Resolution (mm)
4.6	3.1	4.6	4.1

4. RESULTS

To illustrate the effect that gating out the backscatter component has on target contrast as a function of beam attenuation lengths, the contrasts of the WOB and BOW targets were computed for both imaging methods. Furthermore, to investigate the effect that increased forward scatter has on image contrast, two different receiver angular apertures were used for both imaging methods for both targets. The BoW contrast is shown in Figure 6. Although all four cases have similar clear water contrast, it can be seen that the narrow receiver angle (15mrad) CW-LLS images have superior contrast than the wide receiver angle (30mrad) PG-LLS until approximately 5 attenuation lengths, thus suggesting that the contrast reduction due to multiple backscatter dominates the concurrent contrast reduction due to forward scatter for the non-gated system images at beyond 5 attenuation lengths. The narrow receiver angle PG-LLS case, which removes almost all backscatter and significantly reduces forward scatter has superior contrast throughout the entire experiment.

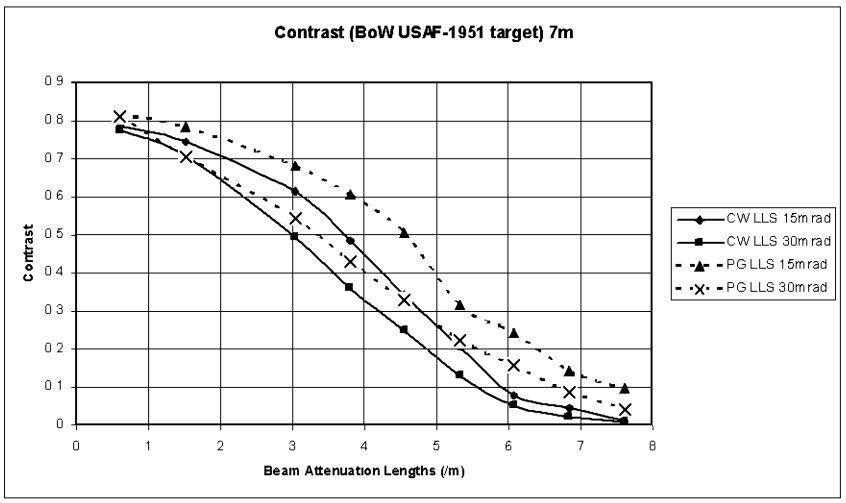

Figure 6. Computed contrast for USAF-1951 Black-on-White target at 7m for CW-LLS versus PG-LLS

Now consider the WoB results in figure 7. It is clear that the lower background reflectance results in a lower forward scatter signal, and the PG-LLS with the wider aperture has a consequent superior contrast to the narrower aperture CW-LLS from 3.5 attenuation lengths onward.

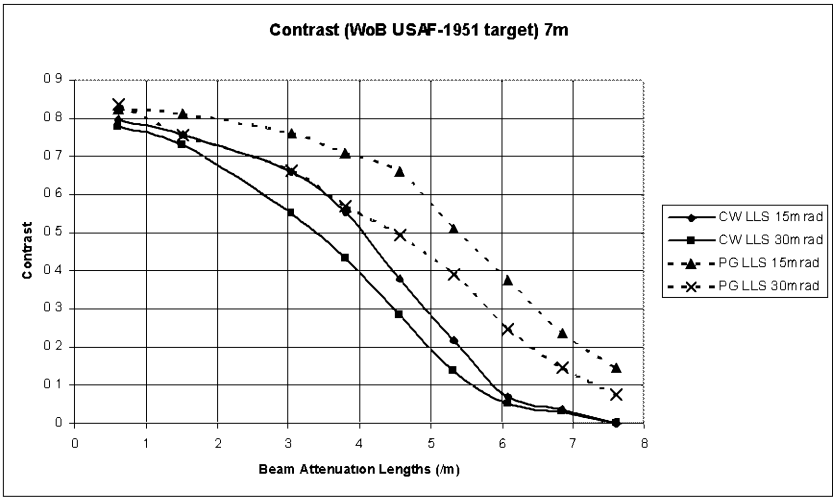

Figure 7. Computed contrast for USAF-1951 White-on-Black target at 7m for CW-LLS versus PG-LLS

This follows from equations 1 and 2, since the CW-LLS image contrast becomes backscatter limited in turbid water (i.e. since the backscatter can not be removed in the CW image, it eventually dominates and washes out the image). The PG-LLS images at 7.6 beam attenuation lengths becomes contrast limited due to forward scatter only when the background reflectance is high, since the backscatter can be substantially reduced by gating, leaving only the forward scatter signal from adjacent regions of the target to limit the contrast. On the other hand, the PG-LLS images with the low reflectance background has a higher contrast in the 7.6 beam attenuation lengths case, and can perhaps be considered approaching power (or photon) limit. In this case, the contrast could be improved with increasing laser pulse energy, whereas for the high reflectance background case the PG-LLS would probably still end up with reaching a contrast limit due to forward scatter. Note that for both the CW-LLS and PG-LLS images the BOW target has a lower contrast than the WoB target. This is due to the fact that the forward scatter degrades the contrast in both cases. This can also be seen from the images. Figure 8 shows the image sequence for the BoW target clearly resulting in the contrast limited case for both the CW-LLS (left hand columns) and PG-LLS (right hand columns) cases, this occurring earlier for the wider aperture cases. Figure 9 shows the WoB image sequences, where the limiting cases clearly show the difference between a contrast limited and a power (or photon) limited regime.

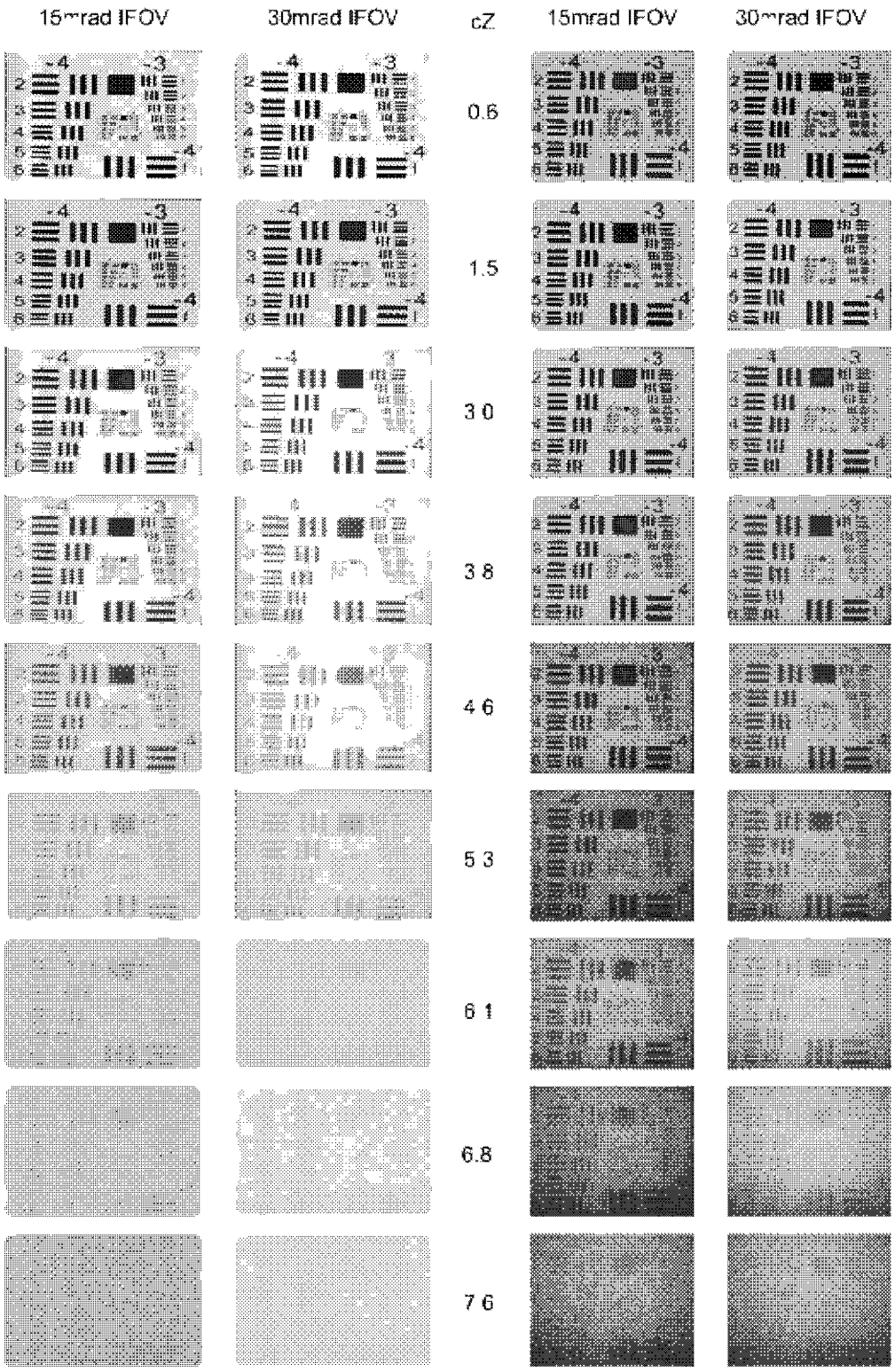

Figure 8. Image sequences from the CW-LLS (left hand columns) and PG-LLS (right hand columns) imagers with the USAF-1951 black-on-white target. Receiver angular aperture (in milliradians) and cZ, the number of attenuation lengths is also shown.

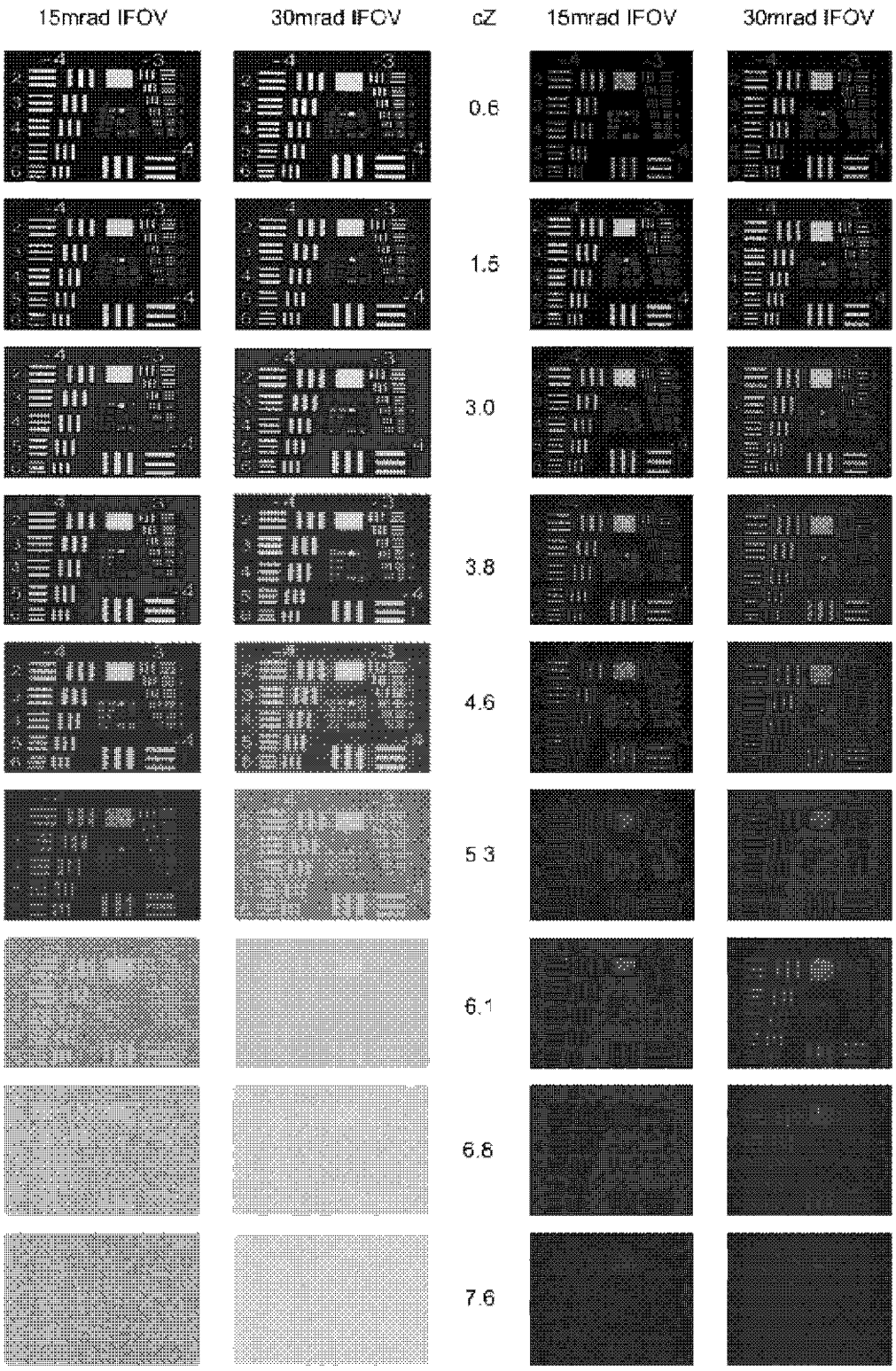

Figure 9. Image sequences from the CW-LLS (left hand columns) and PG-LLS (right hand columns) imagers with the USAF-1951 white-on-black target. Receiver angular aperture (in milliradians) and cZ, the number of attenuation lengths is also shown.

Although the improvement in contrast achievable with the PG-LLS over the CW-LLS is apparent from the images and computed contrast plots, it is also useful to examine how the image noise levels vary between imaging methods as turbidity increases. Figure 10 shows CSNR for the white-on-black target. The initial difference in CSNR between the two imaging methods (from clear water up to 5.5 beam attenuation lengths) is thought to be due to the imperfect energy normalization of the high pulse-to-pulse energy instability. However, the PG-LLS method produces lower noise images beyond 5.5 attenuation lengths for both the light and dark background targets. Between 6.1 and 7.6 attenuation lengths the narrow IFOV PG-LLS configuration produces lower noise images for both targets, particularly the lighter background reflectance (BoW) indicating less forward scattered light entering the receiver.

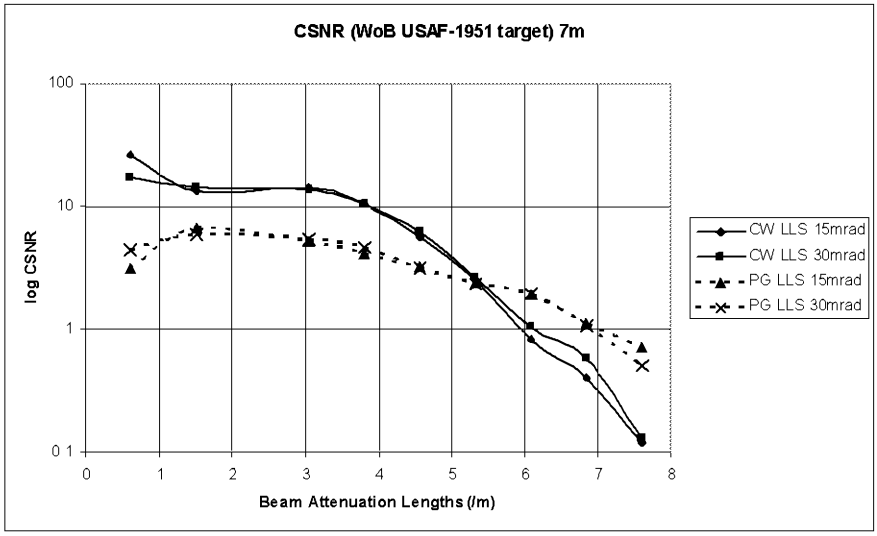

Figure 10. Computed image CSNR for USAF White-on-Black target at 7m for CW-LLS versus PG-LLS

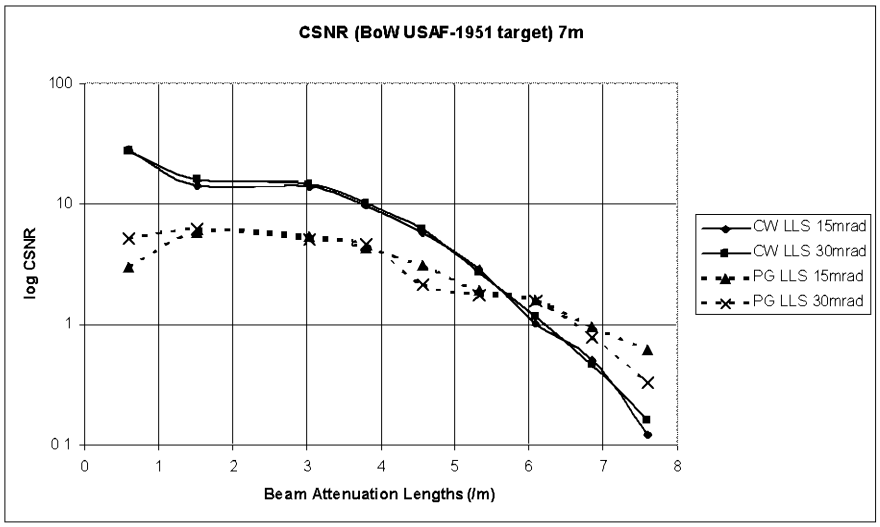

Figure 11. Computed image CSNR for USAF Black-on-White target at 7m for CW-LLS versus PG-LLS

5. CONCLUSIONS

The experimental effort described here demonstrates that the prototype PG-LLS imager is capable of improving image contrast and contrast signal-noise ratio (CSNR) in scattering-dominant waters over that of the existing CW-LLS architecture. Results indicate that for the laser-receiver separation of 23.4cm being investigated with the prototype, the PG-LLS imager becomes limited by forward scattered light at > 7 attenuation lengths instead of reaching a contrast limit due to multiple backscatter at around 6 attenuation lengths in the case of the CW-LLS. Increased laser pulse energy and stability, improvements in gated receiver performance, together the use of processing to isolate acquired pulses from system noise and the tail end of the backscatter signal may further improve performance. Other possibilities involve using laser sources capable of adding modulation to the laser pulse and the use of coherent processing to reject the forward scatter signal mixed within the main pulse envelope, and this is the subject of ongoing work with collaborators. Other funded efforts involve applying developed algorithms to relate the technical target image quality metrics to the ability of human operators to identify small and medium size natural targets from extended range optical imagery.

The larger-scale motivation for this work is to investigate the use of scanned pulsed laser sources with gated receivers for more compact implementations of extended range underwater laser imaging systems than are currently available. An image simulation computer model [14] has also been developed and validated as the main thrust of this work.

6. ACKNOWLEDGEMENTS

This work was conducted under a grant monitored by the US Office of Naval Research.

REFERENCES

[1] Strand, M.P., "Quantitative evaluation of environmental noise in underwater electro-optic imaging systems," Proc. Ocean Optics XIV, Kialua-Kona, HI, (1998).

[2] Kulp, T.J., Garvis, D., Kennedy, R., Salmon, T. and Cooper, K. "Results of the final tank test of the LLNL/NAVSEA Synchronous-Scanning Underwater Laser Imaging System," Proc. Ocean Optics XI, Vol 1750, 453-464. (1992).

[3] Gordon, A. "Turbid test results of the SM2000 laser line scan system and low light level underwater camera tests," Underwater Intervention ' 94: Man and Machine Underwater, Conference Proceedings, Marine Technology Society, 305-311, Washington D.C., (1994).

[4] Strand, M.P., "Underwater electro-optical system for mine identification," Proc. SPIE 2496, 487-497 (1995).

[5] Laux, A., Mullen, L.J., and Cochenour, B., "A Comparison of Extended Range Laser Line Scan Imaging Techniques in Turbid Underwater Environments," Proc. Ocean Optics XIX, Barga, Italy, (2008).

[6] McLean, E.A., Burris, H.R. and Strand, M.P. "Short-pulse range-gated optical imaging in turbid water," Appl. Opt. 34, 4343. (1995).

[7] Swartz, B.A. "Diver and ROV Deployable Laser Range Gated Underwater Imaging Systems," Underwater Intervention '93 Conference Proceedings, New Orleans, Marine Technology Society and Association of Diving Contractors, (1993).

[8] Witherspoon, N.H. and Holloway. J.H. "Feasibility testing of a range-gated laser-illuminated underwater imaging system," Proc. SPIE Int. Soc. Opt. Eng. 1302, 414 (1990).

[9] Fournier, G. R. Bonnier, D. Forand, J. Luc and Pace, P. W. "Range-gated underwater laser imaging system," Opt. Eng. 32, 2185. (1993).

[10] Busck, J. "Underwater 3-D optical imaging with a gated viewing laser radar," Opt. Eng. 44, 116001, (2005).

[11] Caimi, F.M., Dalgleish, F.R., Giddings, T.E. Shirron, J.J., Mazel, C.H., Chiang, K. "Pulse versus CW laser line scan imaging detection methods: simulation results," Proc. Oceans Europe 2007, Aberdeen, Scotland, (2007).

[12] Dalgleish, F.R., Caimi, F.M., Mazel, C.H., Glynn, J.M., Chiang, K., Giddings, T.E. and Shirron, J.J. "Model-based evaluation of pulsed lasers for an underwater laser line scan imager," Proc. Ocean Optics XVIII, Montreal, Canada, (2006).

[13] Dalgleish, F.R., Caimi, F.M., Mazel, C.H. and Glynn, J.M. "Extended Range Underwater Optical Imaging Architecture," Proc. MTS/IEEE Oceans 2006, Boston, MA, (2006).

[14] Giddings, T.E. and Shirron, J.J., "Numerical Simulation of the Electro-Optical Imaging Process in Plane-Stratified Media," submitted to Applied Optics. (2008).